Data-Driven Feedforward Hysteresis Compensation with Genetic Algorithm for Atomic Force Microscope*

Navid Asmari, Mustafa Kangül, Santiago H. Andany, Alireza Karimi, Georg E. Fantner

***Abstract*— Nonlinear dynamics of piezo actuators such as hysteresis, distort the Atomic Force Microscopy (AFM) images as they adversely affect the accuracy of the nano-positioning setup. To compensate for the effects of hysteresis on lateral scanner actuators of AFM, a data-driven feedforward controller design algorithm is proposed. The pair of forward and backward images of a sample are used to extract a mapping between the trace and retrace motion of the actuator. A model corresponding to the input-output mapping of the actuator is defined with a set of unknown parameters. The values of these parameters, which shape the hysteresis curves of the actuator, are optimized through defining and solving an optimization problem. A genetic algorithm is utilized as a tool to look for the optimal values. The hysteresis mapping model is then implemented in the form of an inversion-based feedforward controller to correct the scan waveforms and get matching forward and backward images of the sample. The proposed sensor-less data-driven method is easy to implement as it does not depend on the instrument, the sample under study, or the imaging properties.**

I. Introduction

Scanning Probe Microscopes (SPM) are a family of tools that were developed in the field of nanotechnology with the aim of studying the material surfaces with nanometer resolutions [1]. Atomic Force Microscope (AFM) is a specific SPM instrument designed for scanning surface topographies at nanometer scales. In an AFM, a sharp tip supported on a micro-mechanical cantilever scans the topography of a surface by moving a probe over the surface of the sample and monitoring the interaction between the surface and the probe. Nano-positioning is a vital element of an AFM as it controls the interaction distance between the probe and the sample and creates the raster scan pattern in order to construct an image of the surface topography [2]–[7].

Fig. 1 shows the basic structure of an AFM with a focus on the vertical and lateral scanning actuators. The vertical scanner, the cantilever, the photodiode, and a PID controller constitute a closed-loop, while the lateral scanner is controlled in a separate open-loop or closed-loop scheme. In most of the AFM systems, a raster scan pattern is used to move the tip with respect to the sample and record an image of the sample topography. In this regard, a triangular waveform is sent to one of the lateral scan actuators and the other actuator is commanded with a ramp-shaped signal as shown in Fig. 1. The performance of the AFM highly depends on the characteristics of its individual components, one of which is the nano-positioning stage that performs the scan movements.

Piezo materials are extensively used in AFM scanner systems because of their high resolution and high bandwidth. Despite these advantages, they have linear and nonlinear characteristics that adversely affect the nano-positioning accuracy. The linear dynamics that appear at high scan-rates can be compensated by identification and design of linear controllers correspondingly [6]. The nonlinear dynamics include hysteresis, creep, and changes due to temperature. Hysteresis is one of the nonlinear attributes of the piezo actuators which causes discrepancies between the desired and the achieved motion in the nano-positioning system [8]. Modeling hysteresis in piezoelectric materials has been widely studied [9]–[11] and the developed models have been utilized in nano-positioning systems to adjust the accuracy of the actuators [12], [13].

Either feedback or feedforward controllers can be added to the system to compensate for the effects of hysteresis. In a feedback loop, sensors are added to the system to measure the position of the piezo actuator [14], [15]. However, complex structures, limited bandwidths, added noise, and the high costs of implementation make them unsuitable for some applications. In this regard, a sensor-less feedforward controller can help resolve the problems associated with the actuators' dynamics [16], [17]. The open-loop controllers rely on a model of the actuator which can be quite complex as it should cover a wide-range of dynamics. To overcome the model-dependency problem of the feedforward controller design, a few studies have tried to extract a model by processing AFM images [18], [19].

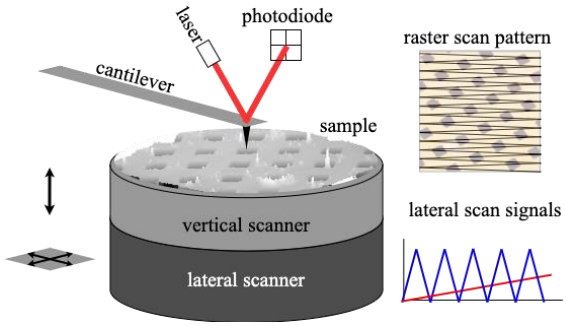

Figure 1. Schematic of the nano-positioning system in a basic AFM setup and the scan pattern and waveforms

Most of these studies depend on special samples to extract the model of the hysteresis. Moreover, many of the proposed models have complex structures to cover for the hysteresis

* Research supported by Swiss Innovation Agency (Innosuisse) and European Research Council (ERC)

N. Asmari†, M. Kangül, S.H. Andany, A. Karimi, G.E. Fantner are with School of Engineering (STI) at Ecole Polytechnique Fédérale de Lausanne (EPFL), 1015 Lausanne, Switzerland

navid.asmari@epfl.ch, mustafa.kangul@epfl.ch, santiago.andany@epfl.ch, alireza.karimi@epfl.ch, georg.fantner@epfl.ch

† corresponding author (navid.asmari@epfl.ch, +41 21 693 53 92)

problem in a general form. We try to alleviate these problems by proposing a hysteresis identification method which can be performed on any sample in AFM imaging, as long as it has sufficient topographic features. By defining a mapping-model of the hysteresis, transforming it into an optimization problem, and solving it efficiently with a genetic algorithm, we reduce the complexity of the problem and prepare a fast framework to identify the effects of hysteresis and design a feedforward controller correspondingly. This easy-to-design feedforward controller can be applied on most of the nano-positioning systems with piezo actuators as it does not require any additional hardware changes.

Using real-time imaging data to extract information about the nonlinear dynamics of the actuators is an appealing idea since it can be extended to a wide range of instruments that are not equipped with sensors. Moreover, a data-driven model of the nonlinear dynamics of the actuators will not depend on the specific instrument or scan properties of the imaging process, which makes it easy-to-implement. We propose an algorithm by which we can create a model of the hysteresis mapping of the actuator. Using the predicted mapping, we design a feedforward controller to compensate for the effects of hysteresis and increase the AFM imaging accuracy. In sections II and III we illustrate how distorted AFM images are used to extract a mapping of hysteresis which goes into the form of an optimization problem. It is followed by section IV where we use the genetic algorithm to solve the optimization problem and find a mapping model of the hysteresis effects which is then validated in section V. In section VI we propose a feedforward controller design using the developed mapping model, and validate it by implementation in an AFM which is discussed in section VII, followed by conclusions and further discussions in section VIII.

II. Problem Definition

The triangular wave applied to a piezo actuator creates a back-and-forth motion on the sample which does not exactly track the command signal. Fig. 2 displays the triangular waveform of the command signal and the corresponding motion of the piezo actuator as it scans one line of the sample topography. Since the actuator is covering (almost) the same area in the trace and retrace motion, in AFM imaging, we can construct two separate images of the same sample area; the forward and the backward images. The difference between the trace and retrace motion of the piezo actuator can be easily observed in the forward and backward images of a sample, as observed in Fig. 3. This difference stems from the hysteresis attribute of the piezo actuator.

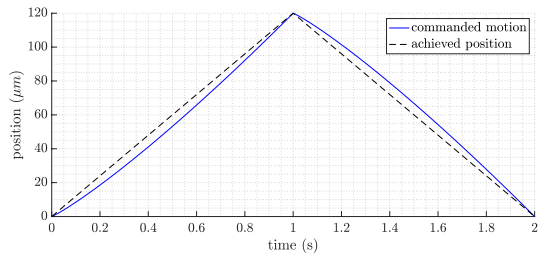

Figure 2. Effect of hysteresis on the lateral scan waveform

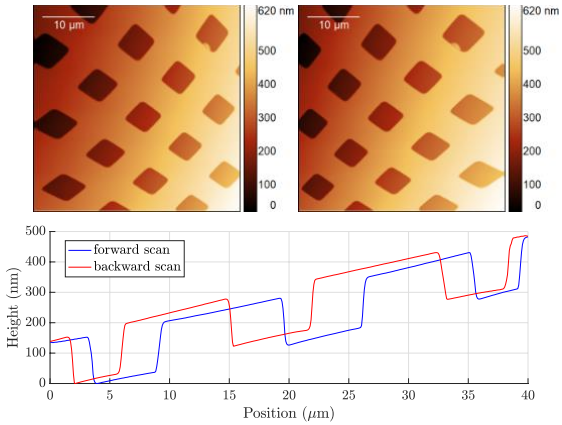

Figure 3. Forward (top left) and backward (top right) height images of a sample consisting of linearly spaced, equal sized pits, and trace (blue) and retrace (red) data for one line of the two images

By building a model of the hysteresis mappings of the actuators, we can design a feedforward controller that compensates for the nonlinearities and helps achieve a more precise image of the sample. Fig. 4 shows the way in which such a feedforward controller can be implemented on the open-loop structure of the lateral scanner. Designing this inversion-based controller relies on having a model of the input-output mappings that are caused by the effects of hysteresis (H) in the actuator. In the following section, we present a procedure by which we can attain this input-output mapping model of the hysteresis by just using the image data.

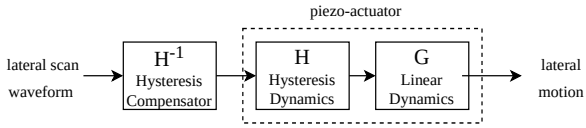

Figure 4. The structure of the feedforward hysteresis compensating controller

III. Data-driven Modeling of Hysteresis Mappings

As the hysteresis attribute of the piezo actuator reveals itself in the forward and backward images, we can use these data to model this nonlinearity. The forward image (U) and the backward image (V) are treated as matrices and u_i and v_j denote the ith and jth columns of the images. Starting with the first column of the forward image, a specific column on the backward image can be correlated with it. Repeating the procedure for all of the columns of the forward image, a vector of trace-retrace mapping (m_{tr}) can be constructed for a specific pair of forward-backward images (Fig. 5).

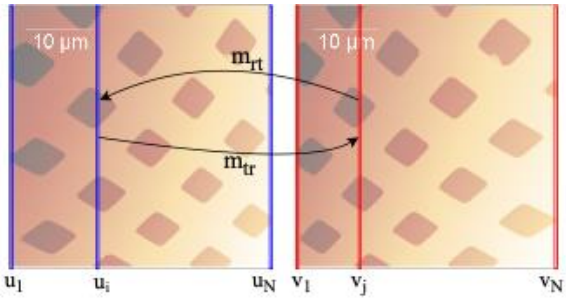

Figure 5. Constructing the mapping between the forward (left) and backward (right) image of a specific sample

Performing the same search for all the columns of the backward image, gives a retrace-trace mapping (m_{rt}) between the same pair of images. As formulated in (1), the mappings from one image direction (forward) to the other (backward) can be constructed by minimizing over the set of its separate columns.

$$\begin{aligned} m_{tr}(i) &= \underset{j}{argmin} \left\| u_i - v_j \right\|_2 \\ m_{rt}(j) &= \underset{i}{argmin} \left\| u_i - v_j \right\|_2 \end{aligned} \tag{1}$$

The results corresponding to the extraction of these mappings for a pair of images are displayed in Fig. 6. The selected pair of images have 512 pixels in each row, which means that the mapping finds the relation between these pixels. The two mappings display the differences in the trace and retrace motions of the actuators with respect to each other. In other words, they are not representing the deviations from the ideal curve, but deviation from one distorted curve to the other.

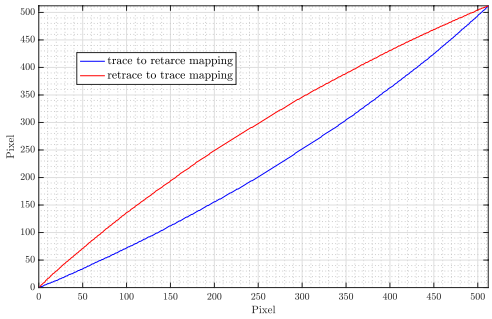

Figure 6. Trace-retrace (m_{tr}) and retrace-trace (m_{rt}) mappings extracted from the pair of images in Fig. 5

In order to extract the hysteresis curves from the mapping data, we first propose a structure for a hysteresis input-output mapping model. In (2), the defined hysteresis mapping is treated as a function, which takes in the requested motion (input command: u_c) and creates the distorted motion of the actuator. The motion is separated into the trace and retrace part, as we know from the observation of the image, that the extending motion of the piezo differs from its contracting motion.

$$h(u_c) = \begin{cases} y_{trace} = f_{\bar{\alpha}}(u_c), & \dot{u}_c \geq 0 \\ y_{retrace} = g_{\bar{\beta}}(u_c), & \dot{u}_c < 0 \end{cases} \tag{2}$$

In this formulation, u_c denotes the normalized commanded motion, which means that it always lies in the [0,1] interval and the two functions, $f_{\bar{\alpha}}$ and $g_{\bar{\beta}}$ represent the normalized achieved motion in the trace and retrace parts, respectively. Although the two functions are different in form, they share some properties. They both pass through the points 0 and 1, and they are both monotonically increasing functions. Having these properties in mind, we define a parametric form for the two functions as shown in (3).

$$\begin{aligned} f_{\bar{\alpha}}(x) &= \left(\sum_{i=1}^{n} x^{\alpha_i} \right) / n = \left(x^{\alpha_1} + x^{\alpha_2} + \ldots + x^{\alpha_n} \right) / n \qquad \alpha_i \geq 1 \\ g_{\bar{\beta}}(x) &= \left(\sum_{i=1}^{n} x^{\beta_i} \right) / n = \left(x^{\beta_1} + x^{\beta_2} + \ldots + x^{\beta_n} \right) / n \qquad \beta_i \geq 1 \end{aligned} \tag{3}$$

The two separate sets of parameters $\bar{\alpha} = \{\alpha_1, \alpha_2, \ldots, \alpha_n\}$ and $\bar{\beta} = \{\beta_1, \beta_2, \ldots, \beta_n\}$ are the unknowns that determine the shape of each function. In order to have the function in the shape which satisfies the mentioned properties of the hysteresis curve, the coefficient of $\bar{\alpha}$ and $\bar{\beta}$ should be greater or equal to 1. This can be added to the problem as a simple constraint. We add another constraint based on the assumption that the actuator takes the same pattern of motion on the trace and retrace motion. The initial points in the trace motion have the same pattern as the initial points in the retrace. The actuator motion looks the same when looked at from the start point to the end point, either on the trace or the retrace. This is equivalent to having trace and retrace motions as mirrored with respect to X and Y coordinates. This constraint relates the functions $f_{\bar{\alpha}}$ and $g_{\bar{\beta}}$ as defined in (4), and it helps eliminate one set of the parameters, either α or β.

$$f_{\bar{\alpha}}(x) = 1 - g_{\bar{\beta}}(1 - x) \tag{4}$$

Looking at a specific command point in the trace direction x^*_{trace}, we know that the actuator will end up at the point y^*_{trace}, this point corresponds to the actual point that the AFM is scanning in the forward image. We know that this same point is scanned in the backward direction, yet, we have to find the command point $x^*_{retrace}$ which takes the scanner to the same position ($y^*_{retrace} = y^*_{trace}$) on the retrace curve. Combining this information with the forms that we assumed for the functions, as formulated in (2) and (3), we can relate the data-driven mappings that were extracted from the images with the functions as defined in (5).

$$\begin{aligned} \tilde{m}_{tr} &= f_{\bar{\alpha}}\left(g_{\bar{\beta}}^{-1}(\bar{x}_c) \right) \\ \tilde{m}_{rt} &= g_{\bar{\beta}}\left(f_{\bar{\alpha}}^{-1}(\bar{x}_c) \right) \end{aligned} \tag{5}$$

In (5), $\tilde{m}_{tr}$ and $\tilde{m}_{rt}$ represent the mappings that are found based on the hysteresis mapping model and $\bar{x}_c$ is a vector of points ranging from 0 to 1. This vector corresponds to all the input points that the function takes as input. A good model should result in calculated mappings $\tilde{m}_{tr}$, $\tilde{m}_{rt}$, that are similar to the measured mappings m_{tr}, m_{rt}. This is the basis of search for the optimal values of the function parameters $\bar{\alpha}$ or $\bar{\beta}$, as formulated in (6).

$$\bar{\alpha}, \bar{\beta} = \underset{}{argmin} \left\| m_{tr} - \tilde{m}_{tr} \right\|_2 \tag{6}$$

This is an optimization problem written based on the trace-retrace mapping, the solution of which gives us the optimal parameters for $\bar{\alpha}$, $\bar{\beta}$. We can write the same optimization problem for the retrace-trace mapping as in (7) noting that it should have the same solution as (6).

$$\bar{\alpha}, \bar{\beta} = \underset{}{argmin} \left\| m_{rt} - \tilde{m}_{rt} \right\|_2 \tag{7}$$

We use the constraint defined in (4) to remove one set of the parameters ($\bar{\beta}$) from the optimization problem. Hence, we end up with a single objective function with a single set of constraints. In the following section, we discuss how we approach solving the optimization problem.

IV. Optimization with the Genetic Algorithm

Considering all the constraints, parameters, and the objective function of the optimization problem, and carrying out the simplifications detailed in section III, we end up with the optimization problem, as summarized in (8).

$$\min_{\bar{\alpha}} \left\| m_{rt} - \left[1 - f_{\bar{\alpha}}\left(1 - f_{\bar{\alpha}}^{-1}\left(\bar{x}_c \right) \right) \right] \right\|_2 \qquad s.t.\ \alpha_i \geq 1 \tag{8}$$

Deriving an analytic solution for the problem is not possible as we have used the inverse of the function that models hysteresis input-output mappings. Instead, we utilize an evolutionary optimization algorithm which solves the problem in a relatively short period of time and does not add to the complexity of the problem. In this regard, the genetic algorithm with a single objective is proposed as a tool for solving the optimization problem [20]. In the following, we provide details about the optimization procedure using the genetic algorithm.

Since we want to minimize the design time for the controller-design part, we start with options that do not add complexity to the problem. In this sense, a population size of 200 is selected. The population is initialized randomly and progresses until the average relative change in the fitness function reaches values less than 1E-6. There is also a limitation on the number of generations with a maximum equal to 100*n, in which n is the number of parameters for $\bar{\alpha}$. This value (n) is a measure of the complexity of the function and is selected based on the values that we can achieve for the fitness function defined in (8). This value highly depends on the actual form of the hysteresis curve and is selected equal to 10. The main reason behind this selection is the marginal improvement in the minimized cost function of the genetic algorithm.

After running the optimization algorithm, we get solutions for $\bar{\alpha}$ which are then used to compute the functions $f_{\bar{\alpha}}$ and $g_{\bar{\beta}}$. Carrying out the optimization process for the data from Fig. 6 we get the optimal values for $\bar{\alpha}$. Substituting these values in (3) and calculating the function for the normalized input range of [0,1] gives the trace and retrace patterns that are plotted in Fig. 7. These are the hysteresis curves of the piezo actuator.

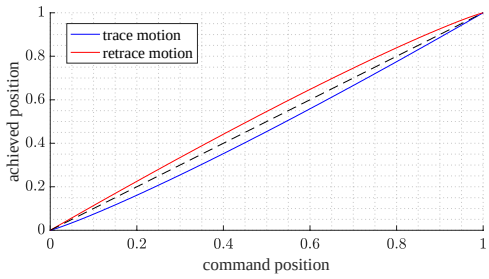

Figure 7. Trace and retrace curves achieved from solving the optimization problem for data from Fig. 6

The optimization results can be verified by comparing the trace-retrace and retrace-trace mappings that were extracted from the image with the ones that are given by (5). In Fig. 8, the mappings that were plotted in Fig. 6 are compared with the results of the optimization. The plot shows that the genetic algorithm has optimized for the parameters based on the defined objective function, which is the resemblance of the extracted and predicted trace-retrace and retrace-trace mappings. The small deviations at the edges correspond to the low degree of the mapping functions. Increasing the order, reduces the discrepancy and increases the complexity without much improvement on the cost function.

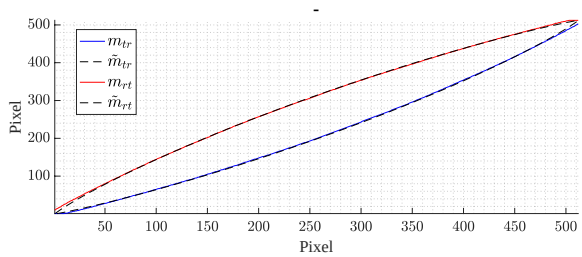

Figure 8. Comparison of the extracted mappings (m_{tr}, m_{rt}) with the predicted mappings ($\tilde{m}_{tr}$, $\tilde{m}_{rt}$) from solving the optimization problem

The whole problem definition process is based on the objective of making both the forward and the backward images look similar to a unique image that corresponds to the actual pattern of the sample topography. In order to reconstruct that original image, we can use the modeled mapping of the hysteresis motion to correct the distorted images back into the original form. In the following section, we present the results on how any hysteresis-distorted pair of forward and backward images can be used to predict the original undistorted form of the image. It should be noted that this post-compensation procedure is not the final goal, but a step to verify the model.

V. Reconstructing the Undistorted Image

The mappings that are extracted from the images based on (1), provide a framework based on which we can convert two images into each other. Rearranging the columns of the forward image (U) based on the trace-retrace mapping (m_{tr}) gives the backward image (V) and vice versa. With the same method of rearranging the columns, we can reconstruct the undistorted image from either the forward or the backward image. In this case, we can use the two hysteresis curve functions $f_{\bar{\alpha}}$ and $g_{\bar{\beta}}$.

The original pair of images from Fig. 5 are rearranged based on the data from Fig. 7 and result in the two images shown in Fig. 9. As observed in this image pair, the trace and retrace topography on each row (horizontal direction), match each other in contrast to what was originally observed in Fig. 5. Since there are no data available for correcting the vertical direction, we assume that both piezo actuators have the same characteristics and use the data from one actuator (in this image configuration, horizontal) on both directions of the image.

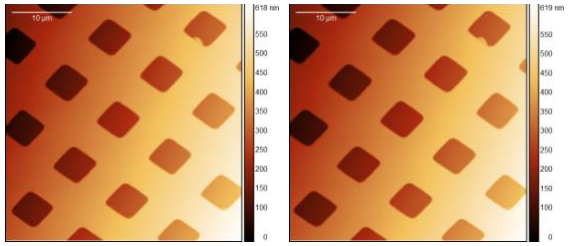

Figure 9. Post-compensating for the effect of hysteresis on forward (left) and backward (right) images (correction on both directions based on the available data)

So far, we have introduced how to create a model that corresponds to the hysteresis input-output mapping and use that model to post-compensate the effects that appear on images. The most important part, though, is to utilize the developed model to design a feedforward controller that can minimize the nonlinear effects of the piezo actuators in the first place (while imaging with the instrument). In the next section, we provide details on designing a feedforward controller based on the data-driven representations that we develop for the hysteresis effects.

VI. Feedforward Controller Design

Since we simplify the hysteresis model as a mapping from input to output, we can invert the simplified model to generate a feedforward controller. As shown in Fig. 4, the command signals are first passed through the controller and the new waveforms are supposed to cover for the hysteresis distortions. This is equivalent to a command-shaping that is carried out through the controller (H^{-1}). Fig. 10 shows the original and hysteresis-compensated waveforms for one of the lateral actuators in a full line-imaging cycle.

The controller design process starts with imaging in the absence of any controller (the scan waveforms are applied to the piezo actuators without any compensation). The forward and backward images of the sample topography are saved and used to extract the trace-retrace mappings based on which, the optimization problem is defined. Solving the optimization problem gives the coefficients that define the shape of the hysteresis mappings. The curves are then inverted to create the function by which the feedforward controller compensates for the effects of hysteresis. It should be noted that the functions generated for different scan sizes differ from each other. In Fig. 11 the hysteresis curves that are generated for different scan sizes are plotted. As observed, the curves do not look the same when we look at them as a mapping function. Despite the differences in the curves, our controller design algorithm will not be affected as it does not depend on the scan size. The data-driven algorithm allows us to design a controller irrespective of the details of the instrument, the sample, or the imaging properties such as speed or size. In the next section, we display the effect of the feedforward controller on the forward and backward images.

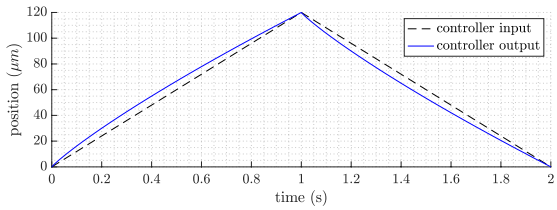

Figure 10. The scan waveforms before (blue) and after (red) compensating for the effects of hysteresis

VII. Imaging with the Feedforward Controller

The designed feedforward controller is implemented on an AFM setup to minimize the effects of hysteresis. In Fig. 12 two sets of images show the uncorrected and corrected scans of the sample. The images on the top row show the forward and backward record of the sample topography when there is no feedforward controller on the loop. The two images at the bottom, show the sample topography when the top images are used to design a controller which is then placed on the loop.

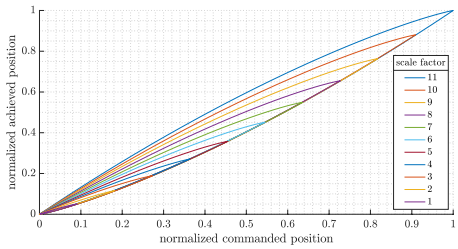

Figure 11. Effect of scan size on the data-driven hysteresis curves (different scale factors represent different scan sizes)

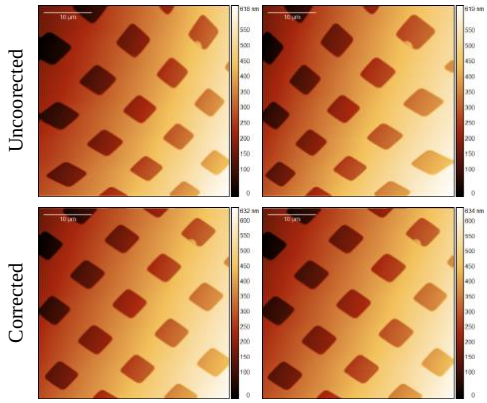

Figure 12. The uncorrected (top) and corrected (below) images in the forward (left) and backward (right) direction of the scan

The controller design process does not depend on the instrument, the scan size, the scan speed, or the sample that is being scanned. Moreover, the design time is as short as a couple of seconds which makes it easy to implement in any kind of experiment. The feedforward controller design is implemented on the setup to scan scratched mica surface and the results are displayed in Fig. 13. In this experiment, the correction on the horizontal direction is performed based on the forward and backward images. To design a controller for the vertical scan direction, we imaged the sample in two different top-to-bottom, and bottom-to-top configurations. The data-driven controller design algorithm is then applied on two different sets of images to compensate for the hysteresis effects of each actuator individually.

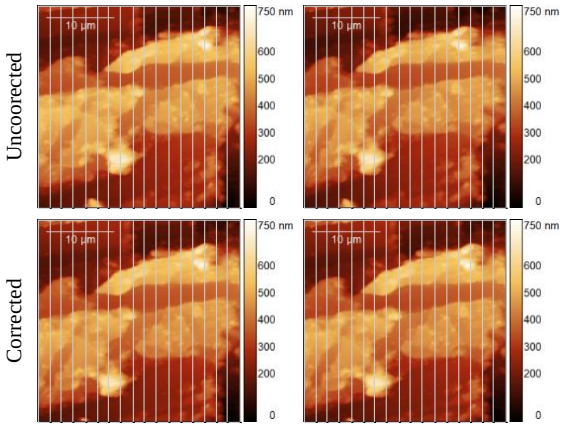

Figure 13. The effect of feedforward controller on backward (left) and forward (right) AFM images of scratched mica sample. The uncorrected images used to model the hysteresis mapping (top) and the corrected images witht the hysteresis compensator (bottom)

Part of the data from Fig. 13, is selected to compare the trace and retrace lines on a specific part of the sample as represented in Fig. 14..

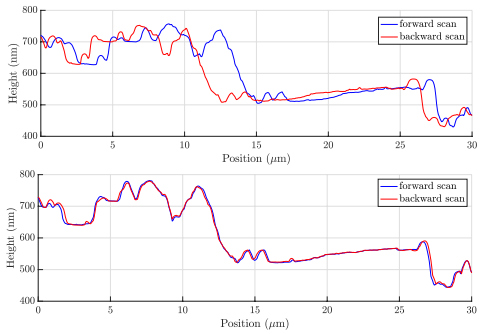

Figure 14. Trace (blue) and retrace (red) topography for one line of the images in the uncorrected (top) and corrected-with-controller (bottom) form corresponding to the images in Fig. 13

VIII. Conclusions

In this article, we propose a data-driven feedforward controller to compensate for the effects of hysteresis on AFM images. We propose an algorithm which takes the hysteresis-distorted images of the AFM as input and creates a model of the hysteresis input-output mappings by generating an optimization problem. A genetic algorithm is utilized as a tool to tackle the problem of solving the optimization problem the parameters of which shape the predicted hysteresis curves. The modeled input-output mappings of actuators are then used to either correct the distorted images or to create an inversion-based controller. The application of the controller on the open-loop configuration of the AFM lateral scanner results in topographies that match on the trace and retrace directions of scan.

One of the advantages of the proposed solution is that it does not require any hardware change which can be complex and expensive in a specific range of instruments. Instead, it relies on the image data that is already at hand. Unlike many other image-based models, the sample topography does not affect the design algorithm as the whole design process does not depend on samples with specific patterns and it does not require large topographies to detect the nonlinearities. The controller design process can be carried out in a few seconds which means that for any specific experiment, it can be repeated. This point makes scan waveform corrections adaptable to any instrument with any imaging configuration on different forms of samples. By carrying out the whole process and implementing it on a setup, we show that implementing the data-driven hysteresis correcting algorithm enhances the AFM images during the imaging process irrespective of the sample topography.

Application of this feedforward controller compensates the effects of hysteresis. A similar approach can be carried out to identify creep and temperature dependent dynamics and compensate them with feedforward controllers.

Acknowledgments

This research was supported by the Swiss Innovation Agency, Innosuisse under grant number 36938.1 IP-EE and the European Research Council, ERC under grant number 588279 InCell/ERC.

References

[1] E. Meyer, H. J. Hug, and R. Bennewitz, Scanning probe microscopy: the lab on a tip. Springer Science & Business Media, 2013.

[2] S. M. Salapaka and M. v Salapaka, “Scanning probe microscopy,” IEEE Control Systems Magazine, vol. 28, no. 2, pp. 65–83, 2008.

[3] Hansma et al., “Tapping mode atomic force microscopy in liquids,” Applied Physics Letters, vol. 64, no. 13, pp. 1738–1740, 1994.

[4] A. P. Nievergelt, S. H. Andany, J. D. Adams, M. T. M. Hannebelle, and G. E. Fantner, “Components for high-speed atomic force microscopy optimized for low phase-lag,” in 2017 IEEE International Conference on Advanced Intelligent Mechatronics (AIM), 2017, pp. 731–736. doi: 10.1109/AIM.2017.8014104.

[5] A. P. Nievergelt et al., “Large-Range HS-AFM Imaging of DNA Self-Assembly through In Situ Data-Driven Control,” Small Methods, vol. 3, no. 7, p. 1900031, 2019.

[6] C. Kammer, A. P. Nievergelt, G. E. Fantner, and A. Karimi, “Data-driven controller design for atomic-force microscopy,” IFAC-PapersOnLine, vol. 50, no. 1, pp. 10437–10442, 2017.

[7] A. P. Nievergelt, B. W. Erickson, N. Hosseini, J. D. Adams, and G. E. Fantner, “Studying biological membranes with extended range high-speed atomic force microscopy,” Sci Rep, vol. 5, no. 1, pp. 1–13, 2015.

[8] D. Croft, G. Shed, and S. Devasia, “Creep, hysteresis, and vibration compensation for piezoactuators: atomic force microscopy application,” J Dyn Syst Meas Control, vol. 123, no. 1, pp. 35–43, 2001.

[9] W. T. Ang, F. A. Garmon, P. K. Khosla, and C. N. Riviere, “Modeling rate-dependent hysteresis in piezoelectric actuators,” in Proceedings 2003 IEEE/RSJ International Conference on Intelligent Robots and Systems (IROS 2003) (Cat. No.03CH37453), 2003, vol. 2, pp. 1975–1980 vol.2. doi: 10.1109/IROS.2003.1248937.

[10] J. Gan and X. Zhang, “A review of nonlinear hysteresis modeling and control of piezoelectric actuators,” AIP Advances, vol. 9, no. 4, p. 40702, 2019.

[11] V. Hassani, T. Tjahjowidodo, and T. N. Do, “A survey on hysteresis modeling, identification and control,” Mech Syst Signal Process, vol. 49, no. 1–2, pp. 209–233, 2014.

[12] Y. Qin, Y. Tian, D. Zhang, B. Shirinzadeh, and S. Fatikow, “A novel direct inverse modeling approach for hysteresis compensation of piezoelectric actuator in feedforward applications,” IEEE/ASME Transactions on Mechatronics, vol. 18, no. 3, pp. 981–989, 2012.

[13] G.-Y. Gu, L.-M. Zhu, C.-Y. Su, H. Ding, and S. Fatikow, “Modeling and control of piezo-actuated nanopositioning stages: A survey,” IEEE Transactions on Automation Science and Engineering, vol. 13, no. 1, pp. 313–332, 2014.

[14] N. Hosseini, A. P. Nievergelt, J. D. Adams, V. T. Stavrov, and G. E. Fantner, “A monolithic MEMS position sensor for closed-loop high-speed atomic force microscopy,” Nanotechnology, vol. 27, no. 13, p. 135705, 2016.

[15] A. Daniele, S. Salapaka, M. v Salapaka, and M. Dahleh, “Piezoelectric scanners for atomic force microscopes: design of lateral sensors, identification and control,” in Proceedings of the 1999 American Control Conference (Cat. No. 99CH36251), 1999, vol. 1, pp. 253–257 vol.1. doi: 10.1109/ACC.1999.782779.

[16] K. K. Leang, Q. Zou, and S. Devasia, “Feedforward control of piezoactuators in atomic force microscope systems,” IEEE Control Systems Magazine, vol. 29, no. 1, pp. 70–82, 2009.

[17] Y. Qin, Y. Tian, D. Zhang, B. Shirinzadeh, and S. Fatikow, “A novel direct inverse modeling approach for hysteresis compensation of piezoelectric actuator in feedforward applications,” IEEE/ASME Transactions on Mechatronics, vol. 18, no. 3, pp. 981–989, 2012.

[18] Y. Zhang, Y. Fang, X. Zhou, and X. Dong, “Image-based hysteresis modeling and compensation for an AFM piezo-scanner,” Asian Journal of Control, vol. 11, no. 2, pp. 166–174, 2009.

[19] Y. Wu, Z. Fan, Y. Fang, and C. Liu, “An effective correction method for AFM image distortion due to hysteresis and thermal drift,” IEEE Transactions on Instrumentation and Measurement, vol. 70, pp. 1–12, 2020.

[20] M. Mitchell, An Introduction to Genetic Algorithms. Cambridge, MA, USA: MIT Press, 1998.